MATEMATIKA, MJIAM, Volume 42, Number 1, 13–32

Flow of Micropolar Hybrid Nanofluid Via Permeable Stretching/Shrinking Sheet and Heat Transfer Optimization Through Response Surface Methodology

[1]Nur Hazirah Adilla Norzawary* [2]Nur Syazana Anuar [3]Norfifah Bachok and [4]Ioan Pop

[1]Institute for Mathematical Research,
Universiti Putra Malaysia, 43400, Selangor, Malaysia.

[2]Faculty of Computer and Mathematical Sciences,
Universiti Teknologi MARA, 40450 Shah Alam, Malaysia.

[3]Department of Mathematics and Statistics, Faculty of Science,
Universiti Putra Malaysia, 43400, Selangor, Malaysia.

[4]Department of Mathematics,
Babes-Bolyai University, 400084 Cluj-Napoca, Romania.

*Corresponding author: nurhazirah.adilla@gmail.com

Article history
Received: 12 November 2024
Received in revised form: 7 Mei 2025
Accepted: 5 June 2025
Published online: 1 April 2026

Abstract Numerical research has been done on the mathematical modelling of micropolar Cu-Al_2O_3/water nanofluid flow driven by a deformable sheet in a stagnation area with suction effect. Using appropriate similarity transformations, the governing partial differential equations are reduced to nonlinear ordinary differential equations, which are then solved numerically using bvp4c function in MATLAB. The hybrid nanofluids are made up of aluminium and copper nanoparticles dispersed in a base fluid called water. Due to variations in numerous relevant parameters, the given problem yields multiple solutions for both shrinking and stretching sheets. Interaction between these input parameters (hybrid nanoparticle, micropolar and suction) and their influences on heat transfer are assessed by a statistical Response Surface Methodology (RSM) model developed by Box–Behnken design approach. The Nusselt number is anticipated to have a maximum value of 18.2903. The RSM results indicate that the highest heat transfer coefficient is achieved when the suction parameter is at its maximum value and the hybrid nanoparticle and micropolar parameters are at their minimum values.

Keywords Dual Solution; Micropolar Fluid; Hybrid Nanofluid; Optimization RSM; Suction.

Mathematics Subject Classification 76N20, 93A30.

1 Introduction

The flow of fluid as it approaches a solid surface and gradually stops at a specific point, called the stagnation point, is known as stagnation point flow. At this point, pressure reaches its maximum and fluid velocity becomes zero. Hiemenz [1] pioneered research into this phenomenon

occurring near a semi-infinite static wall. Meanwhile, micropolar fluid flow has attracted scientific interest due to its applications in polymer fluid extrusion and liquid crystal solidification. Eringen [2] established micropolar fluid theory, which accounts for micro-rotational effects and related inertia. Many researchers have since applied Eringen's concept to various problems. Soid *et al.* [3] studied magnetohydrodynamics (MHD) micropolar fluid flow with slip, incorporating Eringen's ideas, finding that micropolar and slip parameters reduce skin friction coefficient and couple stress when MHD is present. Khashi'ie *et al.*' [4] examined micropolar fluid with mixed convection flow, discovering that stretching flow shows increased surface velocity gradient, local Nusselt, and Sherwood numbers with higher material parameter, unlike shrinking flow. Numerous other studies on micropolar fluid exist [5–11].

The increasing demand for nanofluids in commercial applications has driven extensive research into their properties. Their exceptional ability to enhance heat transfer across various industries including electronics, transportation, and biology has great this interest. Choi and Eastman [12] first introduced nanofluids, which have since been widely applied in solar thermal systems, industrial cooling processes, and many other fields. Researchers like Rahman *et al.* [13], Norzawary *et al.* [14], and Wahid *et al.* [15] have conducted extensive nanofluid research. However, micropolar nanofluids have received relatively little attention. Hussain *et al.* [16] performed numerical studies of micropolar nanofluid on a stretch sheet, finding that increasing nanoparticle volume fraction increases skin friction while decreasing local Nusselt number. Subsequently, Hsiao [[17], Patel *et al.* [18], Lund *et al.* [19], and others have explored various aspects, surfaces, and perspectives of micropolar nanofluid flow problems.

Hybrid nanofluids combine two different nanoparticles with a base fluid, significantly enhancing heat transfer efficiency. Multiple studies [20–26] have shown remarkable improvements in heat conductivity with these innovative fluids. Subhani and Nadeem [1]te27 studied micropolar flow using hybrid (Cu-TiO_2/water) nanofluid, finding that micropolar hybrid nanofluids transfer heat better than standard micropolar nanofluids. Anuar *et al.* [28] researched unsteady flow of micropolar Cu-Al_2O_3/water nanofluid caused by a deformable sheet with radiation effects, discovering that increased unsteadiness and radiation enhance the local Nusselt number, while material parameters have the opposite effect. Norzawary *et al.* [29] studied MHD micropolar hybrid nanofluid flow over a deformable sheet with viscous dissipation, showing that increased material and MHD parameters improve skin friction but reduce the Nusselt number. Despite these findings, micropolar hybrid nanofluid research remains limited. This work aims to investigate how surface stretching and shrinking affect micropolar hybrid nanofluid behaviour.

Numerous researchers have studied the flow and heat transfer of the boundary layer past a stretching/shrinking sheet with applications in manufacturing technology, glass blowing, extrusion of plastic sheets, drawing plastic films, and hot rolling, etc. The outcome quality of the required features is greatly affected by the heat transfer rate along the fluid flow and stretching/shrinking surface. All the fundamental fluid flow problems of a linearstretching/shrinking sheet, the current literature testifies that flow behavior due to a non-linear stretching sheet is also a crucial element in most industrial processes (see Vishalakshi *et al.* [30])

Heat transfer from the plate changes when suction or injection through the boundary surface affects the flow field. Generally, suction increases skin friction and heat transfer, while injection does the opposite [31]. Many researchers have studied these effects in various fluids including carbon nanotubes [32], micropolar fluid [33, 34], and hybrid micropolar fluid [35]. Mahdy *et al.* [36] examined convective flow of micropolar hybrid nanofluid through a permeable

radiating vertical plate in saturated porous medium, considering suction and heat generation effects. They found that increasing suction significantly improved both Nusselt number and skin friction coefficient. Gumber *et al.* [37] investigated natural convective flow of micropolar CuO-Ag/water hybrid nanofluid over a vertical plate in porous media, studying suction/injection effects at the plate's surface. They discovered that injection had a greater impact than suction on temperature distribution and flow velocity. RSM (Response Surface Methodology) combines math and statistics to study problems where multiple independent factors affect a specific outcome. Research has proven RSM's effectiveness across different fields [38, 39]. The method creates regression equations to understand the relationship between input variables and heat transfer rate, aiming to optimize heat transfer. Recently, Wahid *et al.* [40] used RSM to optimize heat transfer in Homann's stagnation-point flow of nanofluids over a shrinking surface. Building on previous research, we aim to study suction effects and expand on Ishak *et al.*'s [5] work by incorporating hybrid micropolar fluid. We'll numerically model fluid flow dynamics and examine how various parameters affect key physical quantities. These numerical results can guide practitioners in experimental and practical applications. We'll also perform RSM statistical analysis and heat transfer optimization. Our work offers a fresh perspective on micropolar hybrid nanofluid contracting properties, with the discovery of non-unique solutions representing a novel contribution to the field.

2 Problem Formulation

Consider a two-dimensional, steady, incompressible stagnation point flow of a micropolar Cu-Al_2O_3/H_2O nanofluid past a stretching or shrinking sheet, as depicted in Figure 1, where are the Cartesian coordinates, with x measured along the sheet, while y is measured in the vertical direction, the flow being in the region $y \geq 0$. In this scenario, both the velocity of the stretch/shrink sheet and the velocity of the fluid in the far-field, denoted by $U_w(x) = ax$ and $U_\infty(x) = bx$, respectively, vary linearly from the stagnation point, where a and $b(> 0)$ are constants.

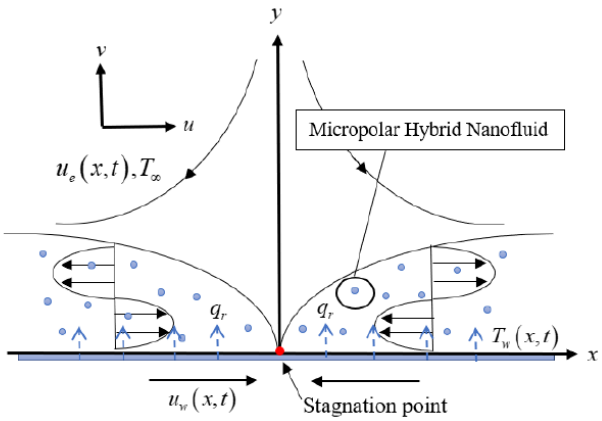

Figure 1: Physical model of shrinking flow.

The governing model for this flow is formulated as presented in [3, 28]:

$$\frac{\partial u}{\partial x}+\frac{\partial v}{\partial y}=0, \tag{1}$$

$$u\frac{\partial u}{\partial x}+v\frac{\partial u}{\partial y}=U_\infty\frac{dU_\infty}{dx}+\frac{\mu_{hnf}+\kappa}{\rho_{hnf}}\frac{\partial^2 u}{\partial y^2}+\frac{\kappa}{\rho_{hnf}}\frac{\partial N}{\partial y}, \tag{2}$$

$$u\frac{\partial N}{\partial x}+v\frac{\partial N}{\partial y}=\frac{\kappa}{\rho_{hnf}j}\left(\frac{\partial u}{\partial y}+2N\right)+\frac{\varsigma}{\rho_{hnf}j}\frac{\partial^2 N}{\partial y^2}, \tag{3}$$

$$u\frac{\partial T}{\partial x}+v\frac{\partial T}{\partial y}=\frac{k_{hnf}}{(\rho C_p)_{hnf}}\frac{\partial^2 T}{\partial r^2}. \tag{4}$$

with the conditions

$$\begin{aligned} &u=U_w, \quad v=V(x), \quad N=-m\tfrac{Cu}{\partial y}, \quad T=T_w \quad \text{at} \quad y=0,\\ &u\to U_\infty, \quad N\to 0, \quad T\to T_\infty \quad \text{as} \quad y\to\infty. \end{aligned} \tag{5}$$

Here (u, v) are the velocities in the direction of and y , N refers to the angular velocity in the xy- plane, T is the temperature of the hybrid nanofluid,κ refers to vortex viscosity,$j = v_f/b$ is density of micro inertial and $\varsigma = (\mu_f+\kappa/2)$ is the spin gradient viscosity [41]. Additionally, m is a constant between [0,1]. When $m = 0$, that also signifies that $N = 0$, the microelements close to the surface cannot spin, which represents concentrated particle flows (Jena and Mathur [42]) or cited in Guram and Smith [43], due to the concentrated microelements. However, the stress tensor anti-symmetric portion dissipates when $m = 0.5$ (low microelements concentration) [41]. Additionally, the situation $m = 1$ is used to describe the flow with turbulence [44].

The subscripts hnf, nf, f, and s denote the physical attributes of hybrid nanofluids, which are also referred to as nanofluid, fluid, and nanoparticle, respectively. Table 1 shows these attributes. The first and second nanoparticles are denoted by $s1$ and $s2$, respectively, and they regulate the volume fraction of Alumina (Al_2O_3), $\varphi_{Al_2O_3}$ and Copper (Cu), φ_{Cu} respectively, with water serving as the base fluid.

Table 1: Physical characteristics of the water-based Cu-Al_2O_3 [18]

Properties	Hybrid nanofluid
Dynamic viscosity	$\frac{\mu_{hnf}}{\mu_f}=(1-\varphi_{Al_2O_3})^{-2.5}(1-\varphi_{Cu})^{-2.5}$
Heat Capacity	$(\rho C_p)_{hnf}=\varphi_{Cu}(\rho C_p)_{s2}+(1-\varphi_{Cu})[(1-\varphi_{Al_2O_3})(\rho C_p)_f+\varphi_{Al_2O_3}(\rho C_p)_{s1}]$
Thermal expansion	$(\rho\beta)_{hf}=\varphi_{Cu}(\rho\beta)_{s2}+(1-\varphi_{Cu}[(1-\varphi_{AI_2O_3})(\rho\beta)_f+\varphi_{AI_2O_3(\rho\beta)_{s1}}])$
Density	$\rho_{hnf}=(1-\varphi_{Cu})[(1-\varphi_{AI_2O_3}\rho_f+\varphi_{AI_2O_3}\rho_{s1}]+\varphi_{Cu}\rho_{s2}$
Thermal conductivity	$\frac{k_{hnf}}{k_{bf}}=\frac{k_{s2}+2k_{bf}-2\varphi_{Cu}(k_{bf}-k_{s2})}{k_{s2}+2k_{bf}+\varphi_{Cu}(k_{bf}-k_{s2})}$ where $\frac{k_{bf}}{k_f}=\frac{k_{s1}+2k_f-2\varphi_{AI_2O_3(k_f-k_{s1})}}{k_{s1}+2k_f-\varphi_{AI_2O_3(k_f-k_{s1})}}$

Additionally, Table 2 provides the thermophysical properties of water, copper, and alumina nanoparticles.

Table 2: Thermophysical properties of the nanoparticles and base fluid [45]

Properties	Water	AI_2O_3	Cu
$C_p\ (J/kgK)$	4179	765	385
$\rho\ (kg/m^3)$	997.1	3970	8933
$k\ (W/mK)$	0.613	40	400

To facilitate the analysis of the current problem, we introduce the following set of similarity variables:

$$\psi = (\upsilon_f b)^{1/2} x f(\eta), \eta = \left(\frac{b}{\upsilon_f}\right)^{1/2}, N = bx\left(\frac{b}{\upsilon_f}\right)^{1/2} h(\eta), \theta(\eta) = \frac{T - T_\infty}{T_w - T_\infty}. \tag{6}$$

Introducing the stream function $u = \frac{\partial \psi}{\partial y}$ and $v = \frac{\partial \psi}{\partial x}$, which satisfy Eq. (1), then Eqs. (1)-(4) and the conditions (5) are written as follows:

$$\left[\frac{\mu_{hnf}/\mu_f}{\rho_{hnf}/\rho_f} + \frac{K}{\rho_{hnf}/\rho_f}\right] f''' + ff'' - f'^2 + 1 + \frac{K}{\rho_{hnf}/\rho_f} h' = 0, \tag{7}$$

$$\left[\frac{\mu_{hnf}/\mu_f}{\rho_{hnf}/\rho_f} + \frac{K}{2(\rho_{hnf}/\rho_f)}\right] h'' + fh' - f'h + 1 + \frac{K}{\rho_{hnf}/\rho_f}(2h + f'') = 0, \tag{8}$$

$$\frac{1}{Pr}\frac{k_{hnf}/k_f}{(\rho C_p)_{hnf}/(\rho C_p)_f}\theta'' + f\theta' = 0, \tag{9}$$

$$\begin{aligned} &f(0) = S, f'(0) = \varepsilon, h(0) = -mf''(0), \theta(0) = 1, \\ &f'(\eta) \to 1, h(\eta) \to 0, \theta(\eta) \to 0, \end{aligned} \tag{10}$$

where $K = \kappa/\mu_f$ is the material parameter, S is the suction parameter and $\epsilon = \frac{a}{b}$is the velocity ratio parameter such that $\epsilon < 0$ is for shrink condition and $\epsilon > 0$ for stretch conditions.

The skin friction coefficient C_f, local couple stress M_w and the local Nusselt number Nu_x are written as

$$\begin{aligned} C_f = \frac{1}{\rho_f U_\infty^2}\left[(\mu_{hnf} + \kappa)\frac{\partial u}{\partial y} + \kappa N\right]_{y=0}, M_w = \frac{1}{\rho_f x U_\infty^2}\left(\mu_{hnf} + \frac{\kappa}{2}\right) j\left(\frac{\partial N}{\partial y}\right)_{y=0}, \\ Nu_x = \frac{-x}{k_f\left(T_f - T_\infty\right)}\left[k_{hnf}\left(\frac{\partial T}{\partial y}\right)\right]_{y=0}. \end{aligned} \tag{11}$$

After performing the transformations, Eq. (11) becomes the following,

$$\begin{aligned} C_f\,\mathrm{Re}_x^{1/2} = \left[\frac{\mu_{hnf}}{\mu_f} + (1-m)K\right] f''(0), \quad M_w\,\mathrm{Re}_x = \left(\frac{\mu_{hvf}}{\mu_f} + \frac{\kappa}{2}\right) h'(0), \\ Nu_x\,\mathrm{Re}_x^{-1/2} = \frac{-k_{hvf}}{k_f}\theta'(0). \end{aligned} \tag{12}$$

3 Analysis of Results and Discussion

3.1 Discussion on Key Findings

Equations (7)–(10) were solved using the bvp4c function in MATLAB. It is noteworthy that during the synthesis of the hybrid nanofluid (Cu-Al_2O_3/water), the process begins with dispersing Al_2O_3/water into water, followed by the addition of Cu. The volume fraction of Al_2O_3/water is fixed at 1%, while the Cu fraction varies from 0% to 2%. The relative tolerance was set to 10^{-10}. A suitable finite value of $\eta \to \infty$, specifically $\eta = \eta_\infty = 10$, was selected. The results comparing $f''(0)$ with previous studies are presented in Table 3, demonstrating a high degree of agreement, which confirms the validity of the numerical results obtained.

Table 3: Values of $f''(0)$ when $\varphi_1 = \varphi_2 = S = 0$, and $m = 0.5$ for $K = 0$ and $K = 1$

ϵ	K=0			K=1		
	Ishak et al. [5]	**Waini et al. [46]**	**Present result**	**Ishak et al. [5]**	**Waini et al. [46]**	**Present result**
0	1.232588	1.232588	1.232588	1.006404	1.006404	1.006404
0.1	1.146561	1.146561	1.146561	0.936163	0.936163	0.936163
0.2	1.051130	1.051130	1.051130	0.858244	0.858244	0.858244
0.5	0.713300	0.713300	0.713300	0.582403	0.582403	0.582403
1	0	0	0	0	0	0
2	-1.887310	-1.887310	-1.887310	-1.540979	-1.540979	-1.540979
5	-10.264750	-10.264750	-10.264750	-8.381133	-8.381133	-8.381133

Figure 2 – Figure 4, Figure 5 – Figure 7, and Figure 8 – Figure 10 depict the skin friction coefficient $C_f Re_x^{1/2}$, local couple stress $M_w Re_x$, and local Nusselt number $Nu_x Re_x^{-1/2}$, respectively, for various values of the suction parameter S, nanoparticle volume fraction parameter φ_{hnf} , and material parameter K. These figures demonstrate that dual solutions exist for the boundary value problem when $\epsilon > 0$ (stretching) and $\epsilon_c < \epsilon < 0$ (shrinking) while no solutions are present when $\epsilon < \epsilon_c$, where ϵ_c represents the critical value.

Figure 2 – Figure 4 illustrate the effects of different S values, showing that as S increases, the range of feasible solutions broadens. Higher suction generally enhances skin friction and heat transfer due to the influence of S, which increases shear stress. A greater S value tends to draw fluid into empty spaces, affecting the surface boundaries. As a result, a rise in temperature stimulates fluid motion, leading to an increase in heat transfer rates. This phenomenon is attributed to the intensified surface shear stress, which extends the boundary layer.

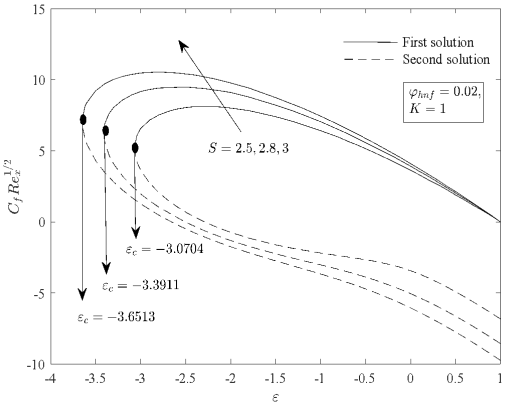

Figure 2: $C_f Re_x^{1/2}$ for different S

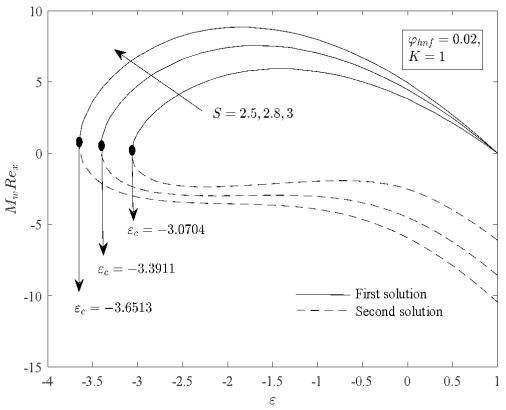

Figure 3: $M_x Re_x$ for different S

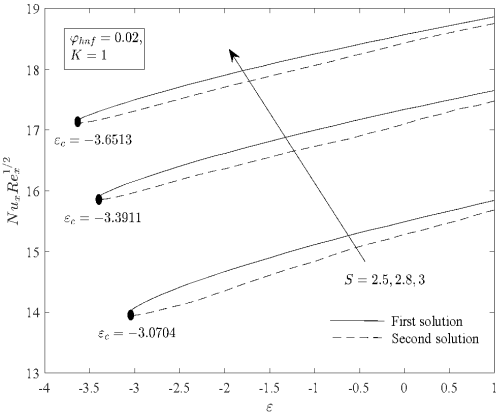

Figure 4: $Nu_x Re_x^{-1/2}$ for different S

Figure 5 – Figure 7 display the plots of $C_f Re_x^{1/2}, M_w, Re_x$ and $Nu_x Re_x^{-1/2}$ for different values of the nanoparticle volume fraction parameter φ_{hnf}. It is observed that both branches of $Nu_x Re_x^{-1/2}$ decrease as φ_{hnf} increases. The addition of nanoparticles significantly raises the fluid's viscosity, resulting in a thicker boundary layer and a reduction in convective heat transfer. Meanwhile, the second branch solutions of $C_f Re_x^{1/2}$ also decrease, but a dual behaviour is noted for the first branch solutions of $C_f Re_x^{1/2}$. In the shrinking region ($\epsilon < 0$), these values increase, while in the stretching region ($\epsilon > 0$), they decrease. Additionally, the figures indicate that the values of $C_f Re_x^{1/2}$ are higher in the shrinking region compared to the stretching region for both branch solutions, whereas the opposite trend is observed for $Nu_x Re_x^{-1/2}$. The increase in fluid viscosity due to nanoparticles leads to a thicker boundary layer, hindering convective heat transfer. It is also evident that as the value of φ_{hnf} rises, the range of feasible solutions expands.

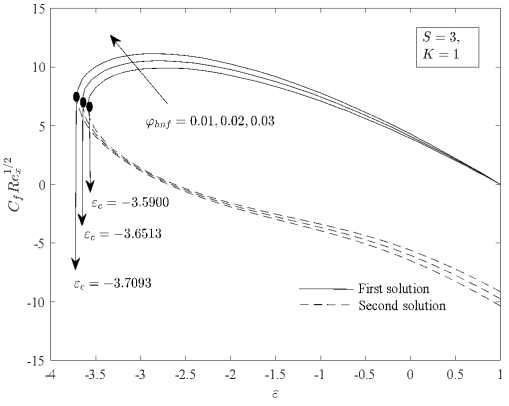

Figure 5: $C_f Re_x^{1/2}$ for different φ_{hnf}

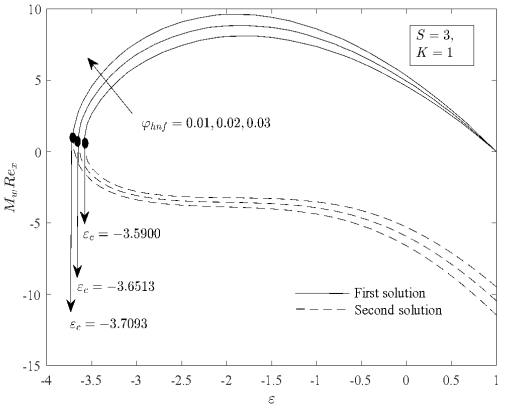

Figure 6: $M_w Re_x$ for different φ_{hnf}

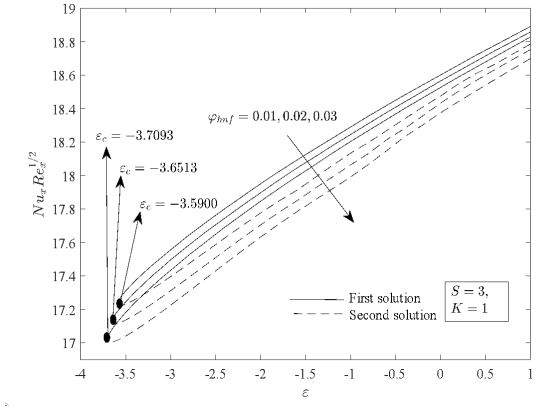

Figure 7: $Nu_x Re_x^{-1/2}$ for different φ_{hnf}

Figure 8 – Figure 10 illustrate that an increase in the micropolar parameter K results in a reduction of $C_f Re_x^{1/2}$ in absolute terms for both shrinking and stretching scenarios. This effect is attributed to the micro-rotation phenomenon, which lowers friction at the fluid-solid interface. Figure 9 shows the couple stress $M_w Re_x$ for different values of micropolar parameter K. The couple stress is related to the gradient of the rotational speed of particles at the surface. For the shrinking plate,$M_w Re_x$ decreases as K increases, whereas for the stretching plate, it increases in absolute terms with rising K. This indicates that as K grows, the micro polarity of the fluid gradually weakens on the shrinking plate due to higher shrinking ratios, while it becomes more pronounced when the plate experiences substantial stretching.

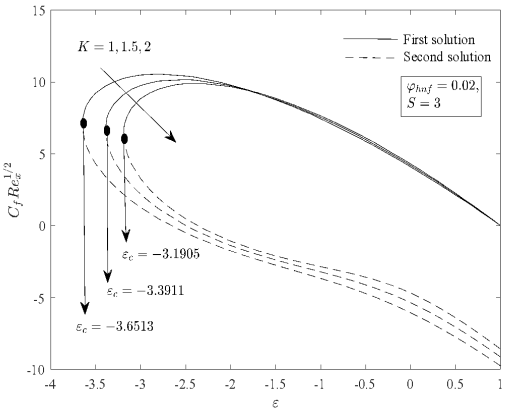

Figure 8: $C_f Re_x^{1/2}$ for different K

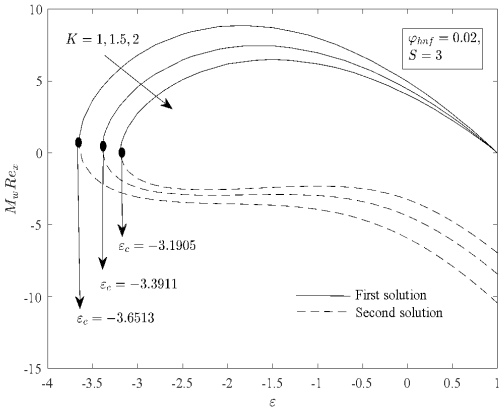

Figure 9: $M_x Re_x$ for different K

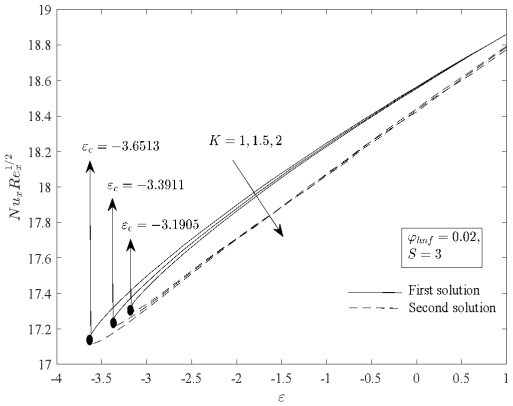

Figure 10: $Nu_x Re_x^{-1/2}$ for different K

Figure 11 – Figure 13 present the momentum, microrotation, and thermal profiles for different values of the suction parameter S. The conformity to far-field boundary conditions confirms the accuracy of the current solutions. Both the first and second solutions show an increasing trend with rising S values, while the temperature profile exhibits an opposite trend. Suction enhances the flow near the plate by reducing the thickness of the momentum boundary layer.

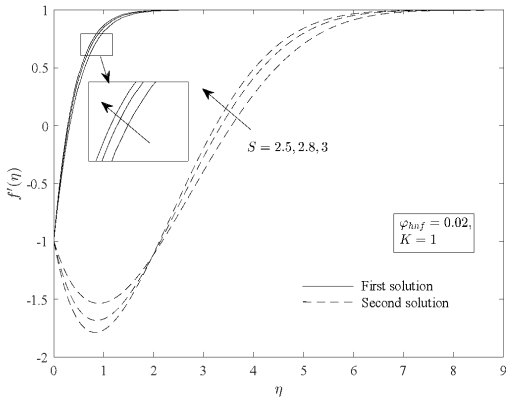

Figure 11: $f'(\eta)$ for varies S

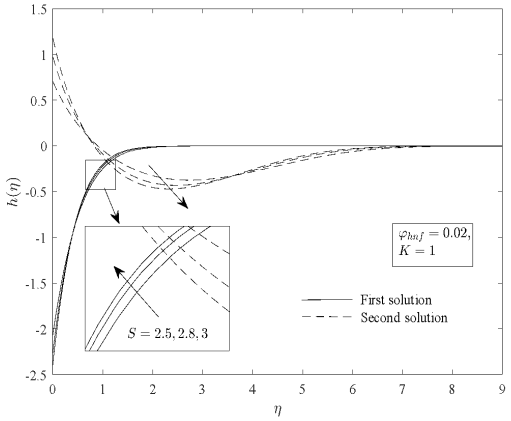

Figure 12: $h(\eta)$ for varies S

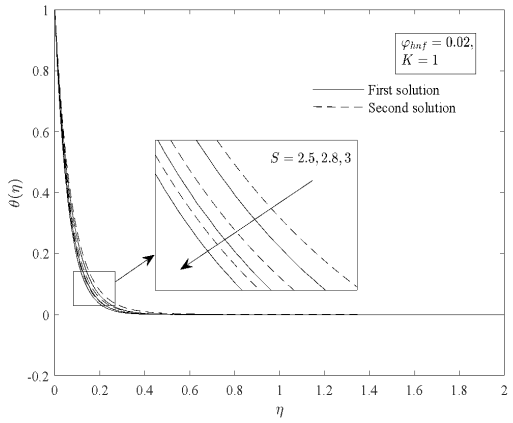

Figure 13: $\theta(\eta)$ for varies S

Figure 14 – Figure 16 illustrate the impact of the nanoparticle volume fraction parameter φ_{hnf} on velocity, microrotation, and temperature profiles. An increase in φ_{hnf} leads to a reduction in the thickness of the momentum and microrotation boundary layers for both solutions. In contrast, the thermal boundary layer thickness expands with higher φ_{hnf} values for both solutions. Additionally, it is evident that the boundary layer thickness of the first solution is thinner than that of the second solution. Furthermore, all the profiles asymptotically satisfy the boundary conditions (10), reinforcing the conclusions drawn from Figure 5 – Figure 7.

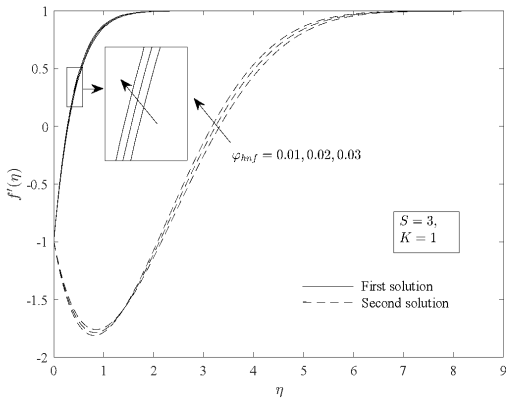

Figure 14: $f'(\eta)$ for varies φ_{hnf}

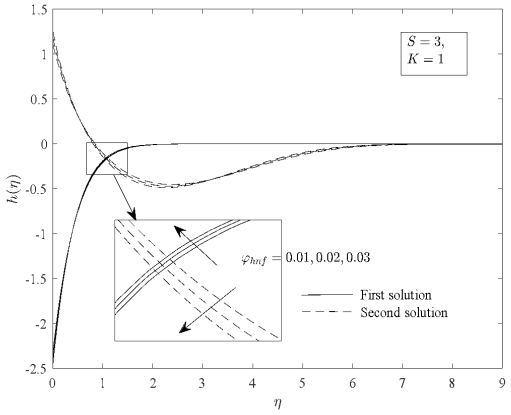

Figure 15: $h(\eta)$ for varies φ_{hnf}

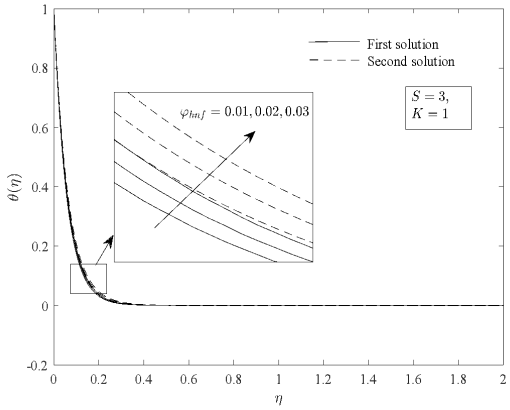

Figure 16: $\theta(\eta)$ for varies φ_{hnf}

3.2 Response surface methodology (RSM)

3.2.1 Response Surface Model Development

The use of response surface methodology (RSM) is a highly effective statistical approach for analyzing and optimizing how key flow field variables affect heat transfer rate ($Nu_x Re_x^{-1/2}$). Within RSM, the face-centered central composite design (CCD), first introduced by Box and Wilson [47], is a notable technique. This study examined how three critical parameters (x_1: hybrid nanoparticle (φ_{hnf}),x_2 : micropolar (K), and x_3: suction (S)) impact heat transfer rate. Table 4 shows the relationship between the three-level codes of these components and the experimental values. The independent factors were coded at three levels: low (-1), medium (0), and high (+1). The number of experimental runs in CCD can be calculated by: $N = k^2 + 2k + C$, where $k = 3$ (number of independent variables) and $C = 6$ (central point). This study conducted 20 runs total, with the experimental data statistically analyzed using Minitab software to determine their effect on heat transfer rate, as shown in Table 5.

Table 4: RSM actual and coded values for input variables

Level	**Actual values**			**Coded levels**
	$x_1 : \varphi_{hnf}$	$x_2 : K$	$x_3 : S$	
Low	0.01	1	2.5	-1
Medium	0.02	1.5	2.8	0
High	0.03	2	3	1

After conducting the CCD analysis, the appropriate input variables for the predictions were identified in a suitable polynomial model. Equation (13) presents the generalized model evaluation equation, which uses a second-order polynomial to predict responses.

$$Y = b_0 + \sum_{i=1}^{n} b_i x_i + \sum_{i=1}^{n} b_{ii} x_i^2 + \sum_{i \neq j=1}^{n} b_{ij} x_i x_j + \gamma \tag{13}$$

where Y represents the predicted response,b_0 is the model intercept,b_i, b_{ii} and b_{ij} are the regression coefficients for the linear, quadratic, and interactive effects of the model, respectively.x_i and x_j are the factors and k is the number of factors.

Table 5: Heat transfer rate experimental design and outcomes when $\epsilon = -1$

Run	Coded Symbols			Uncoded Parameter			Response
	x_1	x_2	x_3	φ_{hnf}	K	S	
1	-1	-1	-1	0.01	1	2.5	15.144871047
2	1	-1	-1	0.03	1	2.5	15.069783917
3	-1	1	-1	0.01	2	2.5	15.122785231
4	1	1	-1	0.03	2	2.5	15.044786344
5	-1	-1	1	0.01	1	3	18.290319518
6	1	-1	1	0.03	1	3	18.202261435
7	-1	1	1	0.01	2	3	18.272680974
8	1	1	1	0.03	2	3	18.182235150
9	-1	0	0	0.01	1.5	2.8	17.023589686
10	1	0	0	0.03	1.5	2.8	16.939336858
11	0	-1	0	0.02	1	2.8	16.992726126
12	0	1	0	0.02	2	2.8	16.972272599
13	0	0	-1	0.02	1.5	2.5	15.094021101
14	0	0	1	0.02	1.5	3	18.235580049
15	0	0	0	0.02	1.5	2.8	16.981291623
16	0	0	0	0.02	1.5	2.8	16.981291623
17	0	0	0	0.02	1.5	2.8	16.981291623
18	0	0	0	0.02	1.5	2.8	16.981291623
19	0	0	0	0.02	1.5	2.8	16.981291623
20	0	0	0	0.02	1.5	2.8	16.981291623

3.2.2 Analysis of variance (ANOVA)

The data presented in Table 6 were used to perform an ANOVA to evaluate the significance of the experiment and examine the factors affecting the heat transfer rate, as detailed in Table 6.

ANOVA assists in determining whether or not statistically significant differences exist between the data categories. The significance criterion is established at a 'P-value' below 0.05, as shown in Table 6. This implies that any parameter whose 'P-value' exceeds this threshold does not contribute significantly to the modelling procedure. Out of the nine model components used for modelling $Nu_x Re_x^{-1/2}$, only one is statistically insignificant. This indicates that practically all of the parameters and the two-by-two combinations are meaningful in predicting the outcome. Therefore, the quadratic term $x_1 * x_1$ is omitted due to the high p-value. Hereafter, the regression equations become:

$$\begin{aligned} Nu_x Re_x^{-1/2} = {} & 16.9813 - 0.041584x_1 - 0.01052x_2 + 1.57068x_3 + 0.001290x_2^2 \\ & + 0.316409x_3^2 - 0.000662x_1x_2 - 0.003177x_1x_3 + 0.001177x_2x_3 \end{aligned} \tag{14}$$

Table 6: ANOVA for RSM utilizing CCD

Source	DF	Adj Sum of Square	Adj Mean Squares	F-value	P-value
Model	9	25.1871	2.7986	27758636.60	0.000
Linear	3	24.6888	8.2296	81628620.58	0.000
x_1	1	0.0173	0.0173	171522.52	0.000
x_2	1	0.0011	0.0011	10977.63	0.000
x_3	1	24.6704	24.6704	2.44703E+08	0.000
Square	3	0.4981	0.1660	1646973.94	0.000
$x_1 * x_1$	1	0.0000	0.0000	0.93	0.358
$x_2 * x_2$	1	0.0000	0.0000	40.64	0.000
$x_3 * x_3$	1	0.2754	0.2754	2732014.59	0.000
2-Way Interaction	3	0.0001	0.0000	315.28	0.000
$x_1 * x_1$	1	0.0000	0.0000	34.82	0.000
$x_2 * x_2$	1	0.0001	0.0001	801.04	0.000
$x_3 * x_3$	1	0.0000	0.0000	109.99	0.000
Error	10	0.0000	0.0000		
Lack-of-fit	5	0.0000	0.0000	*	*
Pure Error	5	0.0000	0.0000		
Total	19	25.1871			

3.2.3 Analysis of response surfaces

Surface response quadratic polynomial models were created to visually show how independent variables affect dependent variables. This process involved changing two independent variables within the experimental range while keeping other components at their mean values, as shown in Figure 17. Figure 17(a) illustrates the interaction between K and φ_{hnf} on heat transfer rate. The response values display a clear gradient, showing that lower hybrid nanoparticle values tend to increase the response. K has a relatively smaller negative impact on heat transfer rate. Figure 17(b) shows the interaction of φ_{hnf} and S on heat transfer rate, revealing that higher suction levels produce higher heat transfer values. A similar pattern is also seen in Figure 17(c).

Additionally, optimization techniques were used to validate the results. One approach involved optimizing heat transfer rate to achieve maximum benefit. The response optimizer in MINITAB software calculated an approximate maximum heat transfer rate of 18.2903 under these conditions: $\varphi_{hnf} = 0.01$ (hybrid nanoparticle), $K = 1$(micropolar), and $S = 3$ (suction). The parameter values recommended for achieving maximum results are consistent with the generated surface and contour plot.

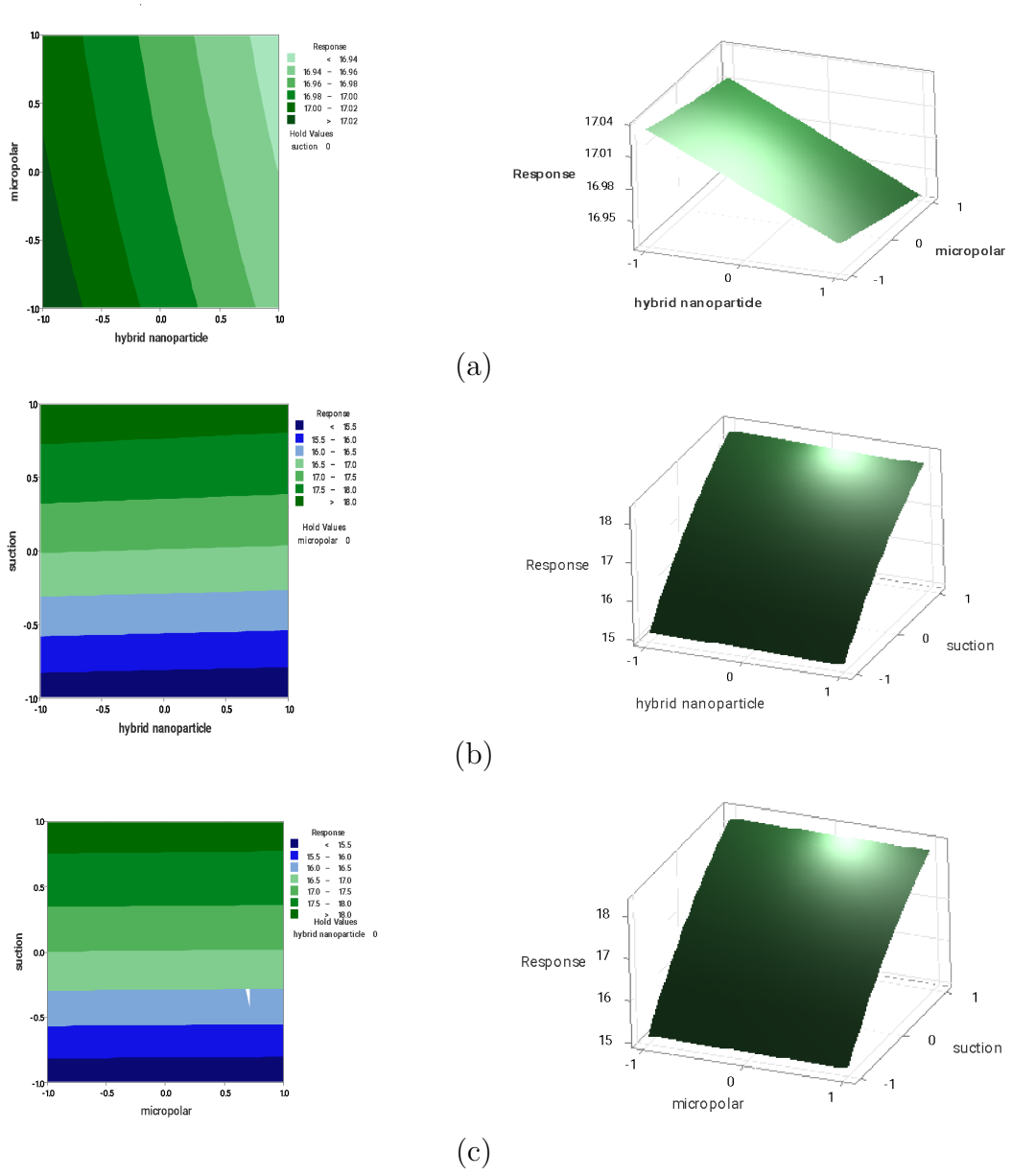

Figure 17: The interaction effect of hybrid nanoparticle, micropolar and suction on $Nu_x Re_x^{-1/2}$

4 Conclusion

This study theoretically examines and analyzes the influence of hybrid nanoparticles, micropolar, and suction parameters on stagnation point flow over a stretching/shrinking sheet. The problem was solved using the MATLAB bvp4c solver. The findings indicate that

- A higher suction parameter typically enhances skin friction and heat transfer.
- An increase in hybrid nanoparticles parameter promotes better skin friction, while decreasing the heat transfer rate.
- As micropolar parameter increases, couple stress $M_w Re_x$decreases for the shrinking plate, while for the stretching plate, it increases.
- The findings from the RSM analysis indicate that increasing the suction parameter to a high value maximises the heat transfer coefficient, while maintaining the hybrid nanoparticle and micropolar parameters at low values.

Acknowledgments

Authors acknowledge the Ministry of Higher Education (MOHE) for funding under the Geran Penyelidikan Fundamental Penyelidik Muda - Early Career Researcher (FRGS-EC/1/2024/STG06/UITM/02/13). The authors wish to thank all the reviewers for their comments and suggestions.

References

[1] Hiemenz, K. (1911). Die Grenzschicht an einem in den gleichformigen Flussigkeitsstrom eingetauchten geraden Kreiszylinder. *Dinglers Polytech. Journal,* 326, 321-324.

[2] Eringen, A. C. (1966). Theory of micropolar fluids. *Journal of mathematics and Mechanics*, 16, 1-18.

[3] Soid, S. K., Ishak, A., & Pop, I. (2018). MHD stagnation-point flow over a stretching/shrinking sheet in a micropolar fluid with a slip boundary. *Sains Malaysiana,* 47(11), 2907-2916.

[4] Khashi'ie, N. S., Md Arifin, N., Nazar, R., Hafidzuddin, E. H., Wahi, N., & Pop, I. (2019). Mixed convective flow and heat transfer of a dual stratified micropolar fluid induced by a permeable stretching/shrinking sheet. *Entropy,* 21(12), 1162.

[5] Ishak, A., Lok, Y. Y., & Pop, I. (2010). Stagnation-point flow over a shrinking sheet in a micropolar fluid. *Chemical Engineering Communications,* 197(11), 1417-1427.

[6] Bhattacharyya, K., Mukhopadhyay, S., Layek, G. C., & Pop, I. (2012). Effects of thermal radiation on micropolar fluid flow and heat transfer over a porous shrinking sheet. *International Journal of Heat and Mass Transfer*. 55, 2945-2952.

[7] Yahaya, R. I., Md Arifin, N., Mohamed Isa, S. S. P., & Rashidi, M. M. (2021). Magnetohydrodynamics boundary layer flow of micropolar fluid over an exponentially shrinking sheet with thermal radiation: Triple solutions and stability analysis. *Mathematical Methods in the Applied Sciences,* 44(13), 10578-10608.

[8] Ahmad, S., Ali, K., Sajid, T., Bashir, U., Rashid, F. L., Kumar, R., & Darvesh, A. (2024). A novel vortex dynamic for micropolar fluid flow in a lid-driven cavity with magnetic field localization–A computational approach. *Ain Shams Engineering Journal,* 15(2), 102448.

[9] Jalili, B., Azar, A. A., Esmaeili, K., Liu, D., Jalili, P., & Ganji, D. D. (2024). A novel approach to micropolar fluid flow between a non-porous disk and a porous disk with slip. *Chinese Journal of Physics,* 87, 118-137.

[10] Srinivasacharya, D., & Reddy, C. R. (2012). Effect of double stratification on mixed convection in a micropolar fluid. *Matematika,* 28(2), 133-149.

[11] Majid, N. A., Mohammad, N. F., Kasim, A. R. M., & Shafie, S. (2019). Forced convective of micropolar fluid on a stretching surface of another quiescent fluid. *Matematika*, 35(3), 397-413.

[12] Choi, S. U., & Eastman, J. A. (1995). *Enhancing thermal conductivity of fluids with nanoparticles*. (No. ANL/MSD/CP-84938; CONF-951135-29). Argonne National Lab.(ANL), Argonne, IL (United States).

[13] Rahman, N. H. A., Bachok, N., & Rosali, H. (2024). MHD Stagnation-point Flow over a Stretching/Shrinking Sheet in Nanofluids. *J. Adv. Res. Fluid Mech. Therm. Sci.*, 76(3), 139–152.

[14] Norzawary, N., Bachok, N., Ali, F., & Rahmin, N. (2022). Double solutions and stability analysis of slip flow past a stretching/shrinking sheet in a carbon nanotube. *Mathematical modeling and computing*, 9, 816-824.

[15] Wahid, N. S., Arifin, N. M., Pop, I., Bachok, N., & Hafidzuddin, M. E. H. (2022). MHD stagnation-point flow of nanofluid due to a shrinking sheet with melting, viscous dissipation and Joule heating effects. *Alexandria Engineering Journal*, 61(12), 12661-12672.

[16] Hussain, S. T., Nadeem, S., & Ul Haq, R. (2014). Model-based analysis of micropolar nanofluid flow over a stretching surface. *The European Physical Journal Plus*, 129, 1-10.

[17] Hsiao, K. L. (2017). Micropolar nanofluid flow with MHD and viscous dissipation effects towards a stretching sheet with multimedia feature. *International Journal of Heat and Mass Transfer,* 112, 983-990.

[18] Patel, H. R., Mittal, A. S., & Darji, R. R. (2019). MHD flow of micropolar nanofluid over a stretching/shrinking sheet considering radiation. *International Communications in Heat and Mass Transfer*, 108, 104322.

[19] Lund, L. A., Omar, Z., Khan, U., Khan, I., Baleanu, D., & Nisar, K. S. (2020). Stability analysis and dual solutions of micropolar nanofluid over the inclined stretching/shrinking surface with convective boundary condition. *Symmetry*, 12(1), 74.

[20] Devi, S. U., & Devi, S. A. (2017). Heat transfer enhancement of Cu-Al_2O_3/water hybrid nanofluid flow over a stretching sheet. *Journal of the Nigerian Mathematical Society*, 36(2), 419-433.

[21] Yahaya, R. I., Arifin, N. M., Nazar, R., & Pop, I. (2020). Flow and heat transfer past a permeable stretching/shrinking sheet in Cu-Al_2O_3/water hybrid nanofluid. *International Journal of Numerical Methods for Heat & Fluid Flow,* 30(3), 1197-1222.

[22] Anuar, N. S., Bachok, N., & Pop, I. (2020). Cu-Al_2O_3/water hybrid nanofluid stagnation point flow past MHD stretching/shrinking sheet in presence of homogeneous-heterogeneous and convective boundary conditions. *Mathematics*, 8(8), 1237.

[23] Kamal, F., Zaimi, K., Ishak, A., & Pop, I. (2019). Stability analysis of MHD stagnation-point flow towards a permeable stretching/shrinking sheet in a nanofluid with chemical reactions effect. *Sains Malaysiana,* 48(1), 243-250.

[24] Ali, Z. M., Ismail, N. Z., Ilias, M. R., Soid, S. K., Ishak, A., Basir, M. F. M., & Norzawary, N. H. A. (2023). Hyperbolic Tangent Fluid Model for Stagnation Flow of Hybrid Nanofluid Over a Stretching Sheet. *Journal of Advanced Research in Fluid Mechanics and Thermal Sciences*, 107(1), 87-101.

[25] Zainal, N. A., Nazar, R., Naganthran, K., & Pop, I. (2020). Unsteady stagnation point flow of hybrid nanofluid past a convectively heated stretching/shrinking sheet with velocity slip. *Mathematics*, 8(10), 1649.

[26] Turkyilmazoglu, M. (2024). Two Models on the Unsteady Heat and Fluid Flow Induced by Stretching or Shrinking Sheets and Novel Time-Dependent Solutions. *ASME Journal of Heat and Mass Transfer*, 146(10).

[27] Subhani, M., & Nadeem, S. (2019). Numerical analysis of micropolar hybrid nanofluid. *Applied Nanoscience,* 9(4), 447-459.

[28] Anuar, N. S., & Bachok, N. (2021). Double solutions and stability analysis of micropolar hybrid nanofluid with thermal radiation impact on unsteady stagnation point flow. *Mathematics*, 9(3), 276.

[29] Norzawary, N. H. A., Soid, S. K., Ishak, A., Mohamed, M. K. A., Khan, U., Sherif, E. S. M., & Pop, I. (2023). Stability analysis for heat transfer flow in micropolar hybrid nanofluids. *Nanoscale advances*, 5(20), 5627-5640.

[30] Vishalakshi, A. B., Mahabaleshwar, U. S., & Sarris, I. E. (2022). An MHD fluid flow over a porous stretching/shrinking sheet with slips and mass transpiration. *Micromachines*, 13(1), 116.

[31] Al-Sanea, S. A. (2004). Mixed convection heat transfer along a continuously moving heated vertical plate with suction or injection. *International Journal of Heat and Mass Transfer*, 47(6-7), 1445-1465.

[32] Norzawary, N. H. A., Bachok, N., & Ali, F. M. (2020). Stagnation point flow over a stretching/shrinking sheet in a carbon nanotube with suction/injection effects. *CFD Letters*, 12(2), 106-114.

[33] Rosali, H., Ishak, A., & Pop, I. (2012). Micropolar fluid flow towards a stretching/shrinking sheet in a porous medium with suction. *International Communications in Heat and Mass Transfer*, 39(6), 826-829.

[34] Sandeep, N., & Sulochana, C. (2015). Dual solutions for unsteady mixed convection flow of MHD micropolar fluid over a stretching/shrinking sheet with non-uniform heat source/sink. *Engineering Science and Technology, an International Journal*, 18(4), 738-745.

[35] Lone, S. A., Alyami, M. A., Saeed, A., Dawar, A., Kumam, P., & Kumam, W. (2022). MHD micropolar hybrid nanofluid flow over a flat surface subject to mixed convection and thermal radiation. *Scientific Reports*, 12(1), 17283.

[36] Mahdy, A., El-Zahar, E. R., Rashad, A. M., Saad, W., & Al-Juaydi, H. S. (2021). The magneto-natural convection flow of a micropolar hybrid nanofluid over a vertical plate saturated in a porous medium. *Fluids*, 6(6), 202.

[37] Gumber, P., Yaseen, M., Rawat, S. K., & Kumar, M. (2022). Heat transfer in micropolar hybrid nanofluid flow past a vertical plate in the presence of thermal radiation and suction/injection effects. *Partial Differential Equations in Applied Mathematics*, 5, 100240.

[38] Wang, J. P., Chen, Y. Z. Ge, X. W. & Yu. H. Q. (2007). Optimization of coagulation–flocculation process for a paper-recycling wastewater treatment using response surface methodology. *Colloids and Surfaces A: Physicochemical and Engineering Aspects*, 302(1), 204–210.

[39] Ghafari, S., Aziz, H. A. Isa, M. H. & Zinatizadeh, A. A. (2009). Application of response surface methodology (RSM) to optimize coagulation–flocculation treatment of leachate using poly-aluminum chloride (PAC) and alum. *Journal of Hazardous Materials*, 163(2), 650–656.

[40] Wahid, N. S., Mustafa, M. S., Arifin, N. M., Pop, I., Anuar, N. S., & Khashi'ie, N. S. (2024). Numerical and statistical analyses of three-dimensional non-axisymmetric Homann's stagnation-point flow of nanofluids over a shrinking surface. *Chinese Journal of Physics*, 89, 1555-1570.

[41] Ahmadi, G. (1976). Self-similar solution of incompressible micropolar boundary layer flow over a semi-infinite plate. *International Journal of Engineering Science,* 14(7), 639-646.

[42] Jena, S. K., & Mathur, M. N. (1981). Similarity solutions for laminar free convection flow of a thermomicropolar fluid past a non-isothermal vertical flat plate. *International Journal of Engineering Science*, 19(11), 1431-1439.

[43] Guram, G. S., & Smith, A. C. (1980). Stagnation flows of micropolar fluids with strong and weak interactions. *Computers & Mathematics with Applications,* 6(2), 213-233.

[44] Peddieson Jr, J. (1972). An application of the micropolar fluid model to the calculation of a turbulent shear flow. *International Journal of Engineering Science*, 10(1), 23-32.

[45] Oztop, H. F., & Abu-Nada, E. (2008). Numerical study of natural convection in partially heated rectangular enclosures filled with nanofluids. *International journal of heat and fluid flow*, 29(5), 1326-1336.

[46] Waini, I., Ishak, A., Lok, Y. Y., & Pop, I. (2022). Micropolar Nanofluid Flow in a Stagnation Region of a Shrinking Sheet with Fe3O4 Nanoparticles. *Mathematics*, 10(17), 3184.

[47] Box, G. E. P., & Wilson, K. B. (1951). On the Experimental Attainment of Optimum Conditions. *Journal of the Royal Statistical Society. Series B. Methodological*, 13(1), 1–38.